



25th International Conference on Fracture and Structural Integrity

Analysis of environmentally assisted cracking processes in notched steels using the point method

Sergio Cicero^{a,*}, Pablo González^a, Borja Arroyo^a, José A. Álvarez^a

^aLADICIM (Laboratorio de la División de Ciencia e Ingeniería de los Materiales), Universidad de Cantabria. ETS Ingenieros de Caminos, Canales y Puertos, Av/Los Castros 44, Santander 39005, España.

Abstract

This paper proposes the use of the Point Method (PM) to analyse Environmentally Assisted Cracking (EAC) processes in steels containing U-shaped notches. The PM, a methodology included within the Theory of Critical Distances (TCD), has been extensively validated by many authors for the analysis of fracture and fatigue phenomena of different types of materials containing notches. However, it has never been applied to other critical or subcritical cracking processes such as EAC or creep crack propagation.

This work provides a PM-based analysis of EAC emanating from notches, which is validated by testing CT notched specimens of X80 and S420 steels subjected to aggressive environments under hydrogen embrittlement conditions.

The results reveal that the PM accurately predicts the crack propagation onset condition, as well as the evolution of the material's apparent EAC resistance.

© 2019 The Authors. Published by Elsevier B.V.

Peer-review under responsibility of the Gruppo Italiano Frattura (IGF) ExCo.

Keywords: Theory of Critical Distances; Point Method; Notch Effect; Environmentally Assisted Cracking; Hydrogen Embrittlement.

1. Introduction

The increasing demand for energy has led to the development of new infrastructures, many of which are located in offshore areas. This offshore environment may cause stress corrosion cracking (SCC) or hydrogen embrittlement

* Corresponding author. Tel.: +34 942 200917; fax: 34 942 201818.

E-mail address: ciceros@unican.es

(HE) phenomena, both of which may lead to brittle failure due to the degradation of the mechanical properties of the materials (e.g., Gangloff (2003)).

In this context, the behavior of steels under SCC or HE conditions is a matter of great importance (e.g., see Koch (2017) and Jones (1996)), given that the repair and replacement of components containing defects in offshore areas (and also in power plants) has become a key issue. Moreover, many structural integrity assessments assume crack-like defects, whereas in practice defects may present a finite radius at their tip (e.g., corrosion defects, mechanical damage, fabrication defects, etc). In such cases, they are referred to as notches, whose assessment as crack-like defects generally leads to overconservative results (e.g., Atzori et al. (2001), Fenghui (2000)).

Nomenclature

Principal symbols

a	crack size
B	specimen thickness
B_N	net specimen thickness
E	Young's modulus
K_{mat}	fracture toughness
K_{mat}^N	apparent fracture toughness
K_{IEAC}	crack propagation threshold for EAC
K_{IEAC}^N	apparent crack propagation threshold for EAC
K_ρ	notch stress intensity factor
K_ρ^c	critical notch stress intensity factor
L	material critical distance
L_{EAC}	material critical distance for EAC
W	specimen width
ρ	notch radius
σ_U	ultimate tensile strength
σ_Y	yield stress
σ_0	inherent strength
σ_{0EAC}	inherent strength for EAC

Principal abbreviations

EAC	Environmentally Assisted Cracking
FEM	Finite Elements
HE	Hydrogen Embrittlement
PM	Point Method
SCC	Stress Corrosion Cracking
TDC	Theory of Critical Distances

Consequently, it is necessary to develop specific methodologies for the analysis of notches. In the last few decades, a group of methodologies capable of predicting the fracture behaviour of notched components has been developed under the name of Theory of Critical Distances (TCD). The different methodologies within TCD employ a characteristic material length parameter, the critical distance (L), when performing fracture and fatigue assessments. The most relevant are the Point Method (PM) and the Line Method (LM), since they are the most simple and they have both been successfully applied in fracture and fatigue analyses (Taylor (2007)). Numerous researchers (e.g., Susmel and Taylor (2007), Madrazo et al. (2014), Justo et al. (2017) have proved the accuracy of the TCD when carrying out fracture and fatigue assessments. However, the TCD has not yet been employed in Environmentally Assisted Cracking (EAC) analyses. The main purpose of this study is to present, through a set of mechanical tests and finite element simulations, an analysis of EAC (Hydrogen Embrittlement in this case) based on the PM. Two steels (X80 and S420), subjected to cathodic polarisation and to two different loading rates, have been

employed in this work. The results show how the PM can predict crack initiation in these two steels when subjected to EAC processes.

2. Theoretical overview: the Point Method and its application to the analysis of EAC processes

2.1. The Point Method

The simplest form of the TCD for performing fracture assessments is the PM. This approach affirms that fracture occurs when the stress at a distance of $L/2$ from the notch tip is equal to the inherent strength, σ_0 . Its mathematical equation is, therefore:

$$\sigma\left(\frac{L}{2}\right) = \sigma_0 \tag{1}$$

Analogously, the PM condition for fatigue assessments follow equation (2):

$$\Delta\sigma\left(\frac{L}{2}\right) = \Delta\sigma_0 \tag{2}$$

where $\Delta\sigma_0$ is the material fatigue limit obtained in plain specimens.

Stress-distance curves at the notch tip in fracture and fatigue assessments are shown in Figure 1. In fracture assessments, the critical distance, L , and the inherent strength, σ_0 , can be obtained by performing two fracture tests on two samples with different radii, as shown in Fig. 1a).

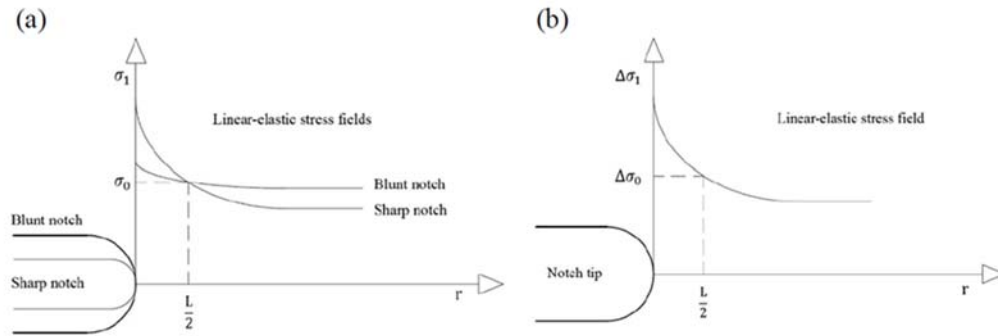


Fig. 1. Obtaining TCD parameters through the stress-distances curves at the notch tip in (a) fracture and (b) fatigue analyses.

The critical distance definition depends on the process being analysed. Thus, in fracture assessments, L follows (Taylor (2007)):

$$L = \frac{1}{\pi} \left(\frac{K_{mat}}{\sigma_0} \right)^2 \tag{3}$$

whereas in fatigue assessments, L follows equation (4):

$$L = \frac{1}{\pi} \left(\frac{\Delta K_{th}}{\Delta\sigma_0} \right)^2 \tag{4}$$

2.2. Hydrogen embrittlement

Hydrogen embrittlement (HE) is a process occurring in metals that is caused by the penetration and the diffusion of atomic hydrogen into the stressed zones of the material (Jones (2014)). As a result, many steels containing hydrogen present premature failures when subjected to tensile stresses. This type of hydrogen damage reduces ductility and is the basic mechanism that controls EAC. In order for HE failure to occur, a susceptible material, an

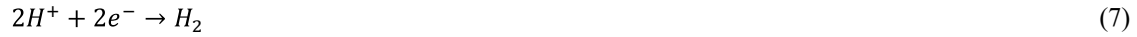
exposure to hydrogen-containing environment, and a high enough stress are simultaneously required. The referred exposure to an aggressive environment involves a corrosion process whose anodic reaction is:



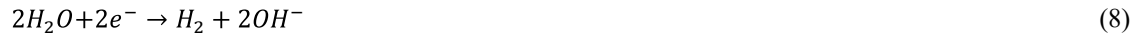
The oxygen is reduced at the metal surface, the cathodic reaction being:



For its part, the cathodic hydrogen evolution in acidic solutions (i.e., pH<4) is:



One of the most widely used methods of corrosion prevention is cathodic protection (or cathodic charge), which reduces the corrosion rate if a potential (or current density) is applied by means of a cathodic polarisation between the anode and the cathode, usually provided by an external source. The main disadvantage of this strategy is that it also increases the H₂ production (Jones (2014)). If the polarisation of the system is excessive, a direct reduction of H₂O is possible:



In such cases, hydrogen causes the breakage of protective layers and damages the metal by HE mechanisms (Hamilton (2011)). Moreover, before the H₂ molecule formation, H atoms are present on the metal surface and can penetrate into interstitial sites causing embrittlement (Shipilov et al. (2008)).

2.3. EAC analysis using the PM

In this work, the PM is applied in the analysis of EAC processes. Thus, the hypothesis is that in order for EAC processes to occur, it is necessary to reach a certain level of stress (σ_{0EAC}) at a distance equal to one half of the material critical distance in EAC conditions (L_{EAC}), which in this case is a constant for a given material, environmental conditions and loading rate. The corresponding equation is:

$$\sigma \left(\frac{L_{EAC}}{2} \right) = \sigma_{0EAC} \quad (9)$$

Analogously to fracture and fatigue analyses, equation (10) is proposed for L_{EAC} :

$$L_{EAC} = \frac{1}{\pi} \left(\frac{K_{IEAC}}{\sigma_{0EAC}} \right)^2 \quad (10)$$

Therefore, when analysing EAC processes in a given material, environment, and loading conditions, the value of L_{EAC} may be determined by testing two specimens with different notch radii and estimating the stress field at the corresponding initiation of crack propagation. Analogously to Figure 1a, the two resulting curves cross each other at a point of coordinates (σ_{0EAC} , $L_{EAC}/2$).

3. Experimental programme

3.1. Materials, environment and loading conditions

This work analyses the application of the PM in two steels: a rolled X80 medium-strength steel (API Specification 5LD (2009)), and a weldable thermo-mechanically treated S420 medium-strength steel (BS EN 10225

(2009)). Their corresponding chemical composition is shown in Table 1, while their tensile properties (as received) are shown in Table 2.

Table 1 Chemical composition of the two steels analyzed (weight %).

	C	Si	S	P	Mn	Ni	Cr	Mo	Cu	Al	V	Ti	Nb
X80	0.07	0.18	<0.005	<0.005	1.83	0.03	-	0.15	0.02	0.03	-	-	0.03
S420	0.08	0.28	0.001	0.012	1.44	0.03	0.02	0.003	0.015	0.036	0.005	0.015	0.031

Table 2. Mechanical properties of the two steels analyzed

Material	E (GPa)	σ_y (MPa)	σ_u (MPa)	e_u (%)
X80	209.9	621.3	692.9	29.6
S420	206.4	447.7	547.1	21.7

In order to generate material embrittlement, cathodic polarisation was used, imposing a fixed current intensity. The steels were connected to the noble metal (platinum) through an aqueous solution at 5mA/cm². The aqueous solution was an acidic electrolyte, prepared following the Pressouyre's method (Bernstein and Pressouyre (1988)), which consists of an 1N H₂SO₄ solution in distilled water with 10mg of an As₂O₃ solution and 10 drops of CS₂ per liter of dissolution. During the test, the pH is kept in the range 0.65-0.80 at room temperature.

Moreover, variables such as loading type and loading rate affect both the crack propagation threshold (K_{IEAC}) and the crack propagation rate (e.g., Gangloff (2003)). In this work, fatigue pre-cracked C(T) specimens and notched C(T) specimens (T-L oriented in both cases) have been tested under the constant displacement method using a slow strain rate machine and following ISO 7539 (2015). Two displacement rates were used: $6 \cdot 10^{-8}$ mm/s and $6 \cdot 10^{-9}$ mm/s. The geometry of the specimens is shown in Figure 2, with the notch radius (ρ) varying from 0 mm (crack-like defect) to 2.0 mm (0 mm, 0.25 mm, 0.50 mm, 1.0 mm and 2.0 mm). Table 3 gathers a summary of the whole experimental programme, composed of 40 C(T) specimens.

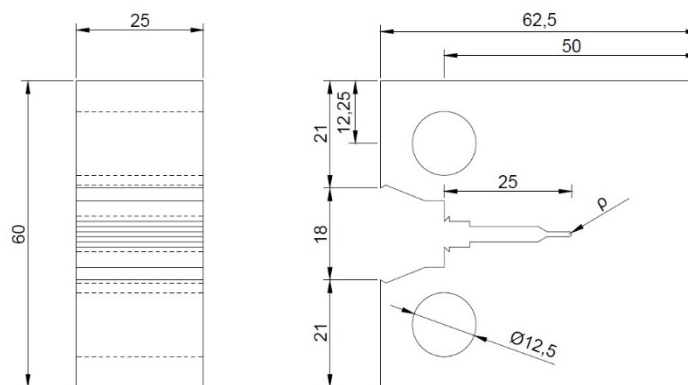


Fig. 2. Geometry of the tested specimens (dimensions in mm).

4. Results and discussion

4.1. Applied loads at crack propagation onset

The specimens were loaded at the different conditions described above, and the corresponding load at the initiation of crack propagation (P_i) was measured. The results are shown in Table 4, where a clear notch effect may

be observed. The effect of the loading rate is moderate in steel X80 and much more significant in steel S420. The table also gathers the final fracture loads (P_c , which took place after crack propagation caused by EAC).

Table 3. Summary of the experimental programme.

Material	Displacement rate (m/s)	ρ (mm)	Number of tests	Displacement rate (m/s)	ρ (mm)	Number of tests
X80	$6 \cdot 10^{-8}$	0.00	2	$6 \cdot 10^{-9}$	0.00	2
		0.25	2		0.25	2
		0.50	2		0.50	2
		1.00	2		1.00	2
		2.00	2		2.00	2
S420	$6 \cdot 10^{-8}$	0.00	2	$6 \cdot 10^{-9}$	0.00	2
		0.25	2		0.25	2
		0.50	2		0.50	2
		1.00	2		1.00	2
		2.00	2		2.00	2

Table 4. Experimental results. a: defect size at crack propagation onset (initial defect length).

Material	Loading rate (m/s)	ρ (mm)	a (mm)	Pi (kN)	Pc (kN)	Material	Loading rate (m/s)	ρ (mm)	a (mm)	Pi (kN)	Pc (kN)
X80	6,0E-08	0,00	28,2	27,86	31,58	S420	6,0E-08	0,00	27,8	28,76	35,07
		0,00	27,4	23,12	24,24			0,00	28,9	24,01	28,71
		0,25	24,0	34,41	37,72			0,25	24,0	34,70	43,23
		0,25	24,0	34,85	40,15			0,25	24,0	33,94	40,66
		0,50	24,0	38,26	40,48			0,50	24,0	37,09	47,91
		0,50	24,0	42,75	49,67			0,50	24,0	34,21	40,71
		1,00	24,0	44,50	47,96			1,00	24,0	41,09	51,69
		1,00	24,0	42,93	55,45			1,00	24,0	40,49	47,13
	2,00	24,0	56,24	63,42	2,00	24,0	45,45	52,98			
	2,00	24,0	54,20	64,90	2,00	24,0	45,67	51,77			
	6,0E-09	0,00	28,6	26,95	27,99	S420	6,0E-09	0,00	29,2	15,71	18,77
		0,00	27,9	26,87	27,99			0,00	28,2	20,66	23,11
		0,25	24,0	34,47	40,36			0,25	24,0	26,41	29,19
		0,25	24,0	35,44	37,92			0,25	24,0	27,57	29,68
		0,50	24,0	39,81	44,85			0,50	24,0	27,59	30,11
		0,50	24,0	38,59	44,81			0,50	24,0	28,21	28,95
1,00		24,0	44,51	53,50	1,00			24,0	30,33	30,88	
1,00		24,0	47,20	51,64	1,00			24,0	28,43	33,06	
2,00	24,0	54,04	59,25	2,00	24,0	37,21	46,35				
2,00	24,0	51,22	52,28	2,00	24,0	35,77	37,08				

4.2. Stress fields at crack propagation onset, and verification of PM methodology

FE simulations were carried out in linear elastic conditions. The structured meshing technique was employed and the models were developed using C3D8R 3D solid elements with a reduced integration. The load applied in the different simulations was the corresponding P_i . Stress fields at the notch tip and stress-distance curves in the central

line of the middle section were obtained, the results being shown in Figures 3 to 6. The stress considered in the analysis is the maximum principal stress.

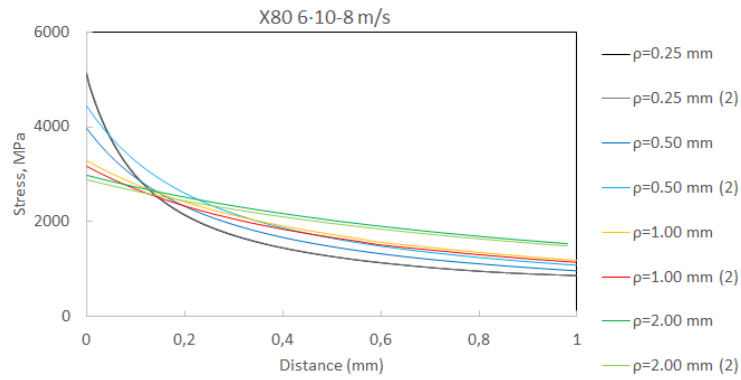


Fig. 3. Stress fields at crack initiation onset. Steel X80, loading rate $6 \cdot 10^{-8}$ m/s.

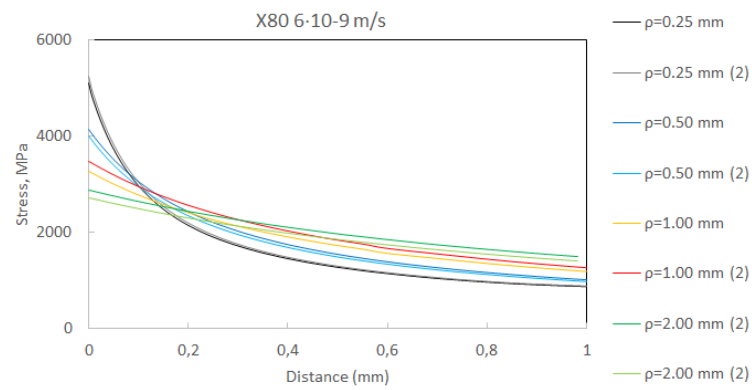


Fig. 4. Stress fields at crack initiation onset. Steel X80, loading rate $6 \cdot 10^{-9}$ m/s.

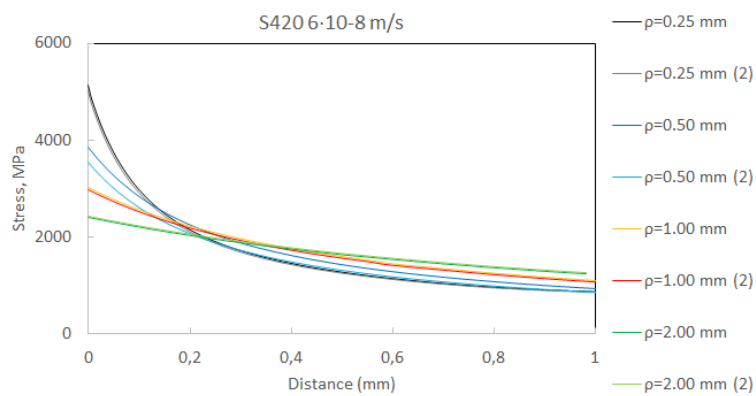


Fig. 5. Stress fields at crack initiation onset. Steel S420, loading rate $6 \cdot 10^{-8}$ m/s.

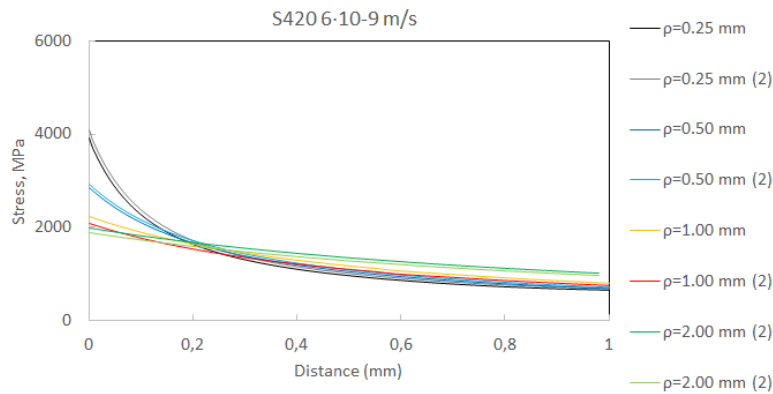


Fig. 6. Stress fields at crack initiation onset. Steel S420, loading rate $6 \cdot 10^{-9}$ m/s.

It can be observed that the different curves cross each other at very proximate points, so the PM hypothesis is fulfilled reasonably well. Considering the average values of the different crossing points identified in each figure, the resulting coordinates ($L_{EAC}/2$, σ_{0EAC}) may be used to derive the corresponding TCD parameters under EAC conditions. The results are summarised in Table 5:

Material	Displacement rate (m/s)	L (mm)	σ_{0EAC} (MPa)
X80	$6 \cdot 10^{-8}$	0.286	2630
	$6 \cdot 10^{-9}$	0.350	2568
S420	$6 \cdot 10^{-8}$	0.462	2101
	$6 \cdot 10^{-9}$	0.452	1589

The results reveal that L is sensitive to the displacement rate in the case of steel X80, with σ_{0EAC} remaining rather constant. On the contrary, L is essentially insensitive to the displacement rate in the case of steel S420, with σ_{0EAC} varying significantly when reducing the displacement rate. All the values of the inherent stress for EAC are much higher than the material tensile strength, suggesting that non-linearity is developed in the process zone.

5. Conclusions

This work analyses the application of the Point Method (PM) to the assessment of crack initiation processes under Environmentally Assisted Cracking (EAC) conditions. The Point Method itself is previously defined in the EAC context.

40 C(T) notched specimens were tested, combining two different materials (X80 and S420), five different radii (from 0 mm up to 2.0 mm), and two different loading rates ($6 \cdot 10^{-8}$ m/s and $6 \cdot 10^{-9}$ m/s). The specimens were all subjected to cathodic polarisation, and submerged in an acidic electrolyte prepared following the Pressouyre's method. In all the tests, the applied load at the crack propagation onset was measured, and the corresponding stress fields at the notch tip were derived from FE analyses. When representing the different stress profiles obtained for each combination of material and loading rate (thus, only varying the notch radius), it was observed that the different curves approximately cross each other at a single point, demonstrating that the PM may be applied to determine the load required for the crack propagation onset under EAC conditions.

Acknowledgements

This work was supported by the Spanish Ministry of Science and Innovation through the research projects MAT2014-58443-P and MAT2014-58738-C3-3-R.

References

- API Specification 5LD, 2009. Specification for CRA Clad or Lined Steel Pipe. American Petroleum Institute, Washington DC.
- Atzori, B., Lazzarin, P., Filippi, S., 2001. Cracks and notches: Analogies and differences of the relevant stress distributions and practical consequences in fatigue limit predictions. *International Journal of Fatigue* 23, 355–362.
- Bernstein, I.M., Pressouyre, G.M., 1988. Role of traps in the microstructural control of hydrogen embrittlement of steels. Noyes Publications, New Jersey.
- BS EN 10225, 2009. Weldable Structural Steels for Fixed Offshore Structures Technical Delivery Conditions. British Standards Institution, London.
- Fenghui, W., 2000. Prediction of intrinsic fracture toughness for brittle materials from the apparent toughness of notched-crack specimen. *Journal of Materials Science* 35, 2543–2546.
- Gangloff, R.P., 2003. Hydrogen assisted cracking of high strength alloys. Aluminum co of America Alcoa Center PA Alcoa Technical Center, Charlottesville.
- Hamilton, J.M., 2011. The challenges of deep-water arctic development. *International Journal of Offshore and Polar Engineering* 21, 241–247.
- ISO 7539, 2015. Corrosion of metals and alloys. Stress corrosion testing. Parts 1 to 11. International Organization for Standardization, Geneva.
- Jones, D.A., 2014. Principles and prevention of corrosion, 2nd ed., New international ed. Harlow, Essex: Pearson.Koch, G., 2017. Cost of corrosion, in “*Trends in Oil and Gas Corrosion Research Technologies*”. In: El-Sherik A.M (Ed.). Woodhead Publishing, Sawston, pp. 3–30.
- Justo, J., Castro, J., Cicero, S., Sánchez-Carro, M.A., Husillos, R., 2017. Notch effect on the fracture of several rocks: Application of the Theory of Critical Distances. *Theoretical and Applied Fracture Mechanics* 90, 251–258.
- Madrazo, V., Cicero, S., García, T., 2014. Assessment of notched structural steel components using failure assessment diagrams and the theory of critical distances. *Engineering Failure Analysis* 36, 104–120.
- Shipilov, S., Jones, R., Olive, J.M., Rebak, R., 2008. Environment-Induced Cracking of Materials. Elsevier, Amsterdam.
- Susmel, L., Taylor, D., 2007. A novel formulation of the theory of critical distances to estimate lifetime of notched components in the medium-cycle fatigue regime. *Fatigue and Fracture of Engineering Materials and Structures* 30, 567–581.
- Taylor, D., 2007. The Theory of Critical Distances: A New Perspective in Fracture Mechanics. Elsevier, Oxford.